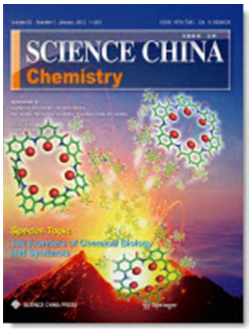

Fabrication of UV responsive micelles-containing multilayers and their influence on cell adhesion

Journal:	*SCIENCE CHINA Chemistry*
Manuscript ID	SCC-2017-0327.R1
Manuscript Type:	Article
Date Submitted by the Author:	n/a
Complete List of Authors:	Zhang, Haolan Wang, Danyu Lin, Xue Politakos, Nikolaos ; CIC biomaGUNE, Biointerfaces Tuninetti, Jimena S. ; CIC biomaGUNE, Biointerfaces Moya, Sergio; CIC biomaGUNE, Biointerfaces Gao, Changyou
Keywords:	Biomaterials, multilayers, surfaces, photo-responsive, cell adhesion
Speciality:	Polymer Sciences

Fabrication of UV responsive micelles-containing multilayers and their influence on cell adhesion

Haolan Zhang[1], Danyu Wang[1], Xue Lin[1], Nikolaos Politakos[2], Jimena S. Tuninetti [2], Sergio Enrique Moya[2]*, Changyou Gao[1,3]*

[1] MOE Key Laboratory of Macromolecular Synthesis and Functionalization, Department of Polymer Science and Engineering, Zhejiang University, Hangzhou 310027, China

[2] Centre for Cooperative Research in Biomaterials, San Sebastian 20009, Gipuzkoa, Spain

[3] Dr. Li Dak Sum & Yip Yio Chin Center for Stem Cell and Regenerative Medicine, Zhejiang University

* Corresponding authors:

Changyou Gao, Prof. Ph.D, email: cygao@mail.hz.zj.cn

Sergio Enrique Moya, Prof. Ph.D, email: smoya@cicbiomagune.es

Abstract:
Multilayers incorporated with stimuli-responsive substances by means of layer-by-layer (LbL) self-assembly are much attractive due to the advantages of stimuli-responsiveness and potential applications in different fields. In this study, pyrenemethyl acrylate (PA) was synthesized, and was copolymerized with acrylic acid (AA) to obtain the amphiphilic and photodegradable P(PA-co-AA) polymers with a PA:AA molar ratio of 1.3:3, and an average molecular weight of 6.9 kDa and polydispersity index of 1.04. They formed micelles spontaneously when dispersed in aqueous solution with a size of 27.5 nm in a dry state and 136.6 nm in a wet state. The micelles were readily decomposed to form aggregates as a result of the cleavage of the pyrenemethyl ester bonds under UV-irradiation. UV-responsive micelles-containing multilayers were prepared by LbL self-assembly of the UV-responsive micelles and polyallylamine hydrochloride (PAH). UV-irradiation of the multilayers resulted in the decomposition of micelles, leading to larger surface roughness, and enhanced swelling ratio and wettability of the multilayers. *In vitro* culture of A549 and HepG2 cells showed significantly better adhesion at 4 h on the UV-illuminated multilayers, whereas the cell proliferation was not affected until 5 d.
Key words: Biomaterials; multilayers; surfaces; photo-responsive; cell adhesion

1. Introduction

The stimuli-responsive biomaterials have witnessed tremendous growth in recent years due to the huge demands in nanotechnology, drug delivery [1-3] and tissue engineering [4, 5]. This type of materials can be triggered by versatile stimuli, including temperature [6], light [2, 7], magnetic field [1] and several chemical [8] or biological [9, 10] signals. Ultra-violet (UV) responsive materials have been widely studied because of their precise control, swift processing and low cytotoxicity [7, 11]. One particular example is materials based on pyrenemethyl ester bond [12, 13], which is cleavable with 365 nm illumination.

Layer by layer (LbL) self-assembly is an effective bottom-up surface functionalization method to construct tailored architectures with multiple composites in nano-scale [14]. The driving forces of LbL self-assembly involve versatile types of interactions between molecules such as electrostatic forces [15], hydrogen bonding [16] and hydrophobic interactions [17]. The multilayers built up by electrostatic interaction between polyelectrolytes, or polyelectrolyte multilayers (PEM), have many applications, especially in the biomedical field [18], for example, protein [15] and cell adhesion [19], drug delivery [20] and biosensors [21]. The composition of multilayers is not restricted to the traditional synthetic polyelectrolytes but also includes proteins, micelles, inorganic nanoparticles and their combinations [15, 21-23]. The self-assembly of amphiphilic copolymers in dilute solutions is widely utilized to fabricate stimuli-responsive micelles or vesicles that are originally intended for drug delivery. Incorporating micelles into PEM by immobilizing them into desired surfaces without losing functions provides an innovation for extending unique properties of micelles into 2D surfaces, which have versatile applications in drug delivery, protein adsorption and cell adhesion [24].

To maintain the advantages of the stimuli-responsive nano-scaled micelles into 2D surfaces, the multilayers incorporated with stimuli-responsive particles by means of LbL self-assembly have been paid much attention in recent years [25-27]. Julia et al. [26] fabricated nanoporous multilayers with reversible pH-triggered swelling transition by self-assembly of pH-responsive block copolymer micelles and polystyrene sulfonate. The swelling degree, morphology and mechanical properties of films are reversibly tuned by solution pH. Zhu et al. [27] reported a type of hydrogen-bonded multilayers composed of temperature-responsive micelles and poly(methacrylic acid). The films are reversibly swollen in response to changes in temperature or salt-concentration as a consequence of collapse or reorganization of the micelle cores.

However, so far there is no attempt to assemble multilayers from photo-decomposable micelles, let alone their manipulation of physiochemical properties and cellular behaviors. Unlike the pH-triggering, the photo illumination is rather green and easily achieved at mild conditions, whereas the structures and properties of multilayers can be manipulated in a wide range. In this work, multilayers are assembled from UV-decomposable poly(pyrenemethyl acrylate-co-acrylic acid) P(PA-co-AA) micelles and poly(allylamine hydrochloride) (Scheme 1). The pyrenemethyl ester bonds in P(PA-co-AA) polymers are easily cleaved by UV irradiation (Scheme 1a) [11], resulting in the release of pyrenemethanol and PAA, and thereby the decomposition of the micelles. This decomposition may further cause the change of multilayer structures and properties such as wettability, swelling property and surface chemical compositions, which in turn bring influences on cell adhesion and proliferation (Scheme 1b). Therefore, A549 and HepG2 cells shall be cultured *in vitro* on the pristine and

UV-illuminated multilayers to compare their cellular behaviors.

2. Experimental

2.1 Materials

1-Pyrenemethanol, acrylate acid (AA), 3-(4,5-dimethyl-thiazol-2-yl)-2,5-diphenyltetrazolium bromide (MTT) and 4',6-diamidino-2-phenylindole (DAPI) were purchased from Sigma-Aldrich. Acryloyl chloride (AC), triethylamine (TEA), azobisisobutyronitrile (AIBN) and poly(allylamine hydrochloride) (PAH) were purchased from TCI. Dulbecco's Modified Eagle's Medium (DMEM) was purchased from Gibco. Fetal bovine serum (FBS) was purchased from Sijiqing. Bovine serum albumin (BSA), streptomycin and penicillin were purchased from Beyotime Biotechnology. Calcein AM was purchased from Yeasen. Rhodamine-labeled phalloidin was purchased from Invitrogen. Other chemicals were of analytical grade and used as received. The water used in all experiments was purified by a Millipore Milli-Q system, and has a resistivity higher than 18.2 MΩ·cm.

2.2 Fabrication of photoresponsive micelles-containing multilayers

Pyrenemethyl acrylate was synthesized by a reaction between pyrenemethanol and acryloyl chloride (AC). In brief, 2.32 g (10 mmol) pyrenemethanol and 4.2 mL (30 mmol) TEA were dissolved in 100 mL tetrahydrofuran (THF). A solution of 2.45 mL (30 mmol) AC in 20 mL THF was added dropwise under agitation at 0-5 ^{o}C. The reaction was then maintained at room temperature for 24 h. The resulted mixture was filtered to obtain the filtrate, which was dried under reduced pressure. It was dissolved in dichloromethane and washed with saturated sodium bicarbonate aqueous solution for several times to remove acrylic acid. Then the organic phase was evaporated, and the residue was recrystallized in ethanol and dried under vacuum at 40 ^{o}C. Finally, the pyrenemethyl acrylate (PA) was obtained with a yield of 77%.

Poly(pyrenemethyl acrylate-co-acrylic acid) (P(PA-co-AA)) was synthesized by copolymerization of PA and AA. 286 mg (1 mmol) PA, 274 μl (4 mmol) AA, and 22.96 mg (2.8%, mol ratio, AIBN:C=C) AIBN were dissolved in 1,4-dioxane, and reacted under nitrogen atmosphere at 60-70 ^{o}C for 8 h. After the mixture was dried under reduced pressure, the obtained product was dissolved in THF. Precipitate was obtained by adding excess of cold hexane, which was dried in vacuum at 40 ^{o}C. P(PA-co-AA) was obtained with a yield of 31%.

To prepare photoresponsive P(PA-co-AA) micelles, P(PA-co-AA) was dissolved in THF with a concentration of 1 mg/mL, which was then added dropwise into a 5-fold 0.1 M NaCl aqueous solution under ultrasonic dispersion. The solution was then agitated (500 rpm) at room temperature for 1 h. After the pH value was adjusted to 7.0 and followed with dialysis against 0.1 M NaCl aqueous solution for 1 d in a dialysis tube, the photodegradable pyrene-containing micelles were obtained.

Photo-responsive micelles-containing multilayers were fabricated by LbL self-assembly of P(PA-co-AA) micelles and PAH. In brief, glass slides, silica substrates and quartz substrates were cut into a size of 1.5×1 cm, soaked in piranha solution (70% H_2SO_4+30% H_2O_2) overnight, washed with plenty of Millipore water, and finally dried in a 60 ^{o}C oven. The cleaned substrates were first dipped in

0.2 mg/mL PAH/0.1M NaCl solution with a pH value of 7.0 for 5 min, washed with Millipore water for 3 times, and dried with a nitrogen flow. The substrates were then dipped in the micelles-containing solution with a concentration of 0.2 mg/mL for 5 min, washed with Millipore water for 3 times, and dried with a nitrogen stream. The multilayers were obtained by repeating the above steps alternatingly, and are referred as pristine multilayers. For all the characterizations and applications, 6 bilayers were assembled except of the monitoring of thickness increase by UV-vis spectroscopy.

2.3 Photo-irradiation of the micelles and multilayers

The photoinduced transformation of micelles and multilayers were carried out by illuminating micelles solution or multilayers soaked in certain amount of water with 365 nm wavelength light source (50 mW/cm^2) for 5 min.

To confirm the photo-responsiveness and to determine the extent of transformation induced by UV illumination, the multilayers assembled on quartz substrates were illuminated for different time, and were then incubated in ethanol for 30 min to dissolve the dissociated pyrenemethanol in the multilayers. Then the UV-vis spectroscopy was used to determine the remained pyrene in the multilayers.

2.4 Characterizations

^1H nuclear magnetic resonance spectra (NMR) were measured by a Brucker DMX500 equipment by using dimethyl sulfoxide-d_6 (DMSO-d_6) as the solvent. UV-vis absorbance spectra were measured by a Shimadzu UV-2550 spectrophotometer. Fourier transform infrared spectra (FTIR) were measured by Brucker TENSOR II. The molecular weight and weight polydispersity index (PDI) were characterized by a Waters 1515 gel permeation chromatography (GPC) setup at 60 ^oC by using poly(methyl methacrylate) standards for calibration and THF as eluent. The size and zeta potential of the micelles were measured by dynamic light scattering (DLS) with a Zetasizer Nano-ZS from Malvern Instruments. Transmission electron microscopy (TEM) was measured by JEM-1230. The wettability of the multilayers was analyzed by a static water contact angle measurement system (DSA 100, Krüss, Germany) using a sessile-drop method. The volume of each droplet was 2 μL, and each measurement was repeated for 3 times. The surface morphology and thickness of the films were measured by atomic force microscopy (AFM) with a Nanoscope V Multimode Atomic Force Microscope, Bruker. For the thickness analysis, each sample was scratched with a pipette tip previously. Images were acquired in a tapping mode using oxide-sharpened silicon nitride tips for air measurement and antimony-doped Si tips for liquid (in Milli-Q water) measurement. Results were analyzed with Gwyddion software.

2.5 Cell experiments

A549 and HepG2 cell lines were obtained from the Cell Bank of the Chinese Academy of Sciences (Shanghai, China), and were maintained in DMEM supplemented with 10% FBS, 100 μg/mL streptomycin, and 100 U/mL penicillin at 37 °C in a 5% CO_2 humidified incubator (Forma Series II, Thermo Fisher Scientific Inc., USA).

For the cell adhesion experiments, after labeled with 4 μL/10ml Calcein AM, A549 and HepG2 cells

were seeded on different surfaces at a density of 1.1×10^4 cell/cm^2. After 4 h incubation, the substrates were gently rinsed with phosphate buffered saline (PBS) 3 times to wash off unattached cells. The cells on different surfaces were recorded under a fluorescence microscope (IX81, Olympus). At least 10 images were randomly recorded and 3 paralleled samples were conducted. The numbers were counted with Image Pro Plus software.

To determine the cell viability, 20 μL MTT (5 mg/mL) was added to each well after certain time periods of incubation on different substrates, and the cells were continuously cultured at 37 °C for 4 h. Dark blue formazan crystals generated by mitochondria dehydrogenase in viable cells were dissolved in dimethyl sulfoxide (DMSO) to measure the absorbance at 570 nm using a microplate reader (Tecan infinite M200Pro). Three parallel experiments were conducted.

Cell actin organization and nucleus were visualized after fluorescent staining. Cells were seeded at a density of 1.1×10^4 cells/cm^2 and incubated for 4 h, and then were fixed with 4% paraformaldehyde at 37 °C for 30 min. Next, they were washed with PBS 3 times and treated with 0.5% Triton X-100 for 5 min. After being washed with PBS 3 times again, the samples were incubated in a 1% BSA/PBS solution for 1 h. After washed twice, the cells were stained with DAPI and rhodamine-labeled phalloidin for 1 h. After washed 3 times in PBS, the cells were observed under a confocal laser-scanning microscope (CLSM, LSM-510, Zeiss).

2.6 Statistical analysis

Statistical analysis was performed based on one-way analysis of variance (ANOVA) with a Tukey post hoc method. A significance level of $p < 0.05$ was chosen for all the tests. A few comparisons were also made between individual groups via t-test with the same significant level.

3. Results and discussion

3.1 Synthesis and characterization of P(PA-co-AA) copolymers

To prepare the amphiphilic and photo-responsive polymers, the key monomer, pyrenemethyl acrylate (PA) was synthesized by the reaction between pyrenemethanol and acryloyl chloride (AC) under 0-5 ^{o}C. In Fig. 1a, the peaks of ^{1}H NMR at 6.00, 6.27 and 6.28ppm (No.2,3,4) are assigned to protons of the ethylene groups. Signals of methylene groups at 5.95 ppm (No.1) and aromatic rings between 8.13 and 8.38 ppm (No.5) refer to the structure of pyrene methyl groups. The integral ratio of peaks No.5:1:2:3:4 was 9.21:2.02:1:1:1.04, which had a good accordance with that of protons in pyrenemethyl acrylate (9:2:1:1:1), proving the successful synthesis of pyrenemethyl acrylate.

Next, the P(PA-co-AA) copolymers were synthesized by radical polymerization of PA and AA, whose structure was also characterized by ^{1}H NMR (Fig. 1b). The peaks between 5.44 and 5.91 ppm (No.1), and 7.65 and 8.41 ppm are assigned to protons of methylene and aromatic rings of pyrenemethyl groups, which had a similar integral ratio (9.1:2) to protons of corresponding structures (9:2). However, the similar structures of PA and AA units lead to overlapping of peaks of protons in the backbone between 1.25 and 3.60 ppm. The amount of AA units can hardly be quantified by peak at 12.32 ppm either because of the swift exchange between reactive hydrogen of carboxyl groups and hydrogen of water.

Compared the FTIR spectra of PA, AA and P(PA-co-AA) copolymers (Fig. 1c), the absorbance at 1000-983cm^{-1} referring to the C=C of PA disappeared in the P(PA-co-AA) spectrum, revealing the

success of copolymerization. The existing peaks of C-O-C at 1245 and 1172cm^{-1} confirmed the reservation of ester bonds.

Moreover, the copolymer ratio of PA: AA was quantified as 1.3:3 by UV-vis spectroscopy by referring to a standard curve of pyrenemethanol at 342 nm (data not shown). The molecular weight (Mn) and PDI of the copolymers was measured by GPC, which were 6.9 kDa and 1.04, respectively.

3.2 Preparation of P(PA-co-AA) micelles and their photoresponsive transformation

The P(PA-co-AA) micelles with an average size of 27.5 nm and a spherical morphology (Fig. 2a) were easily formed by diluting the P(PA-co-AA)/THF solution with 0.1 M NaCl aqueous solution. They had a larger hydrodynamic diameter of 136.6 nm with a PDI of 0.17 in water (Fig. 2c). The high swelling ratio of the micelles, which was 5.0 calculated by the ratio of sizes from DLS and TEM, suggests the strong hydration rate due to the repulsive force of carboxylate groups, as confirmed by the negative zeta potential of -21.6±1.1 eV.

After illumination by UV, the spherical micelles (Fig. 2a) were transformed into irregularly shaped aggregates (Fig. 2b), with an increase of the average size to 201 nm and a broadened PDI to 0.26 (Fig. 2d). When illuminated by UV, the micelles were decomposed into water-soluble poly(acrylic acid) and pyrenemethanol as a result of the breaking of the pyrenemethyl ester bonds. The released pyrenemethanol is rather hydrophobic, and thus self assembles into larger aggregates via hydrophobic interaction and π-π stacking.

3.3 Photoinduced transformation of micelles-containing multilayers

Next, these photo-decomposable and negatively charged micelles were used as a building block to assemble multilayers with positively charged PAH. The increase of absorbance in 250-400 nm, which includes several specific absorbance peaks of pyrene, demonstrates the stepwise assembly of the multilayers (Fig. 3a). Taking into account the linear absorbance at 343 nm vs bilayer number, one can conclude that the multilayers were built up in a linear pattern too. This result is similar to the growth law of PAA/PAH multilayers in other research [28], which shows linear growth of PAA/PAH in pH between 6.0 and 8.0.

Photo-decomposition of the micelles in the multilayers was demonstrated by UV-vis spectroscopy too (Fig. 4). After the multilayers were illuminated with UV for 30 s, they were incubated in ethanol for 30 min to dissolve the released pyrenemethanol. Compared with the pristine sample, there was a sharp decrease in absorption of the photo-irradiated multilayers between 250 to 400 nm (Fig. 4a). The same ethanol treatment to the pristine multilayers did not bring significant weakening of the absorption, revealing the good stability of micelles in the multilayers and pyrenemethyl ester bonds against ethanol (good solvent for pyrenemethanol). Fig. 4b shows the remnant absorbance at 343 nm as a function of the UV-irradiation time, demonstrating that the decomposition took place in a very fast rate. 30s illumination resulted in over 50% cleavage of the pyrenemethyl bonds, and 300 s was long enough to decompose almost completely the micelles. Hence, this irradiation time was chosen for all the next experiments to prepare the UV-illuminated films.

After illuminated by UV, the surface roughness of multilayers increased from 0.60 nm (Fig. 5a) to 1.68 nm (Fig. 5b), which is contributed from the transformation of micelles to aggregates formed by the released pyrenemethanol. The thickness of multilayers was measured by AFM in both dry and wet

states (Fig. 6) by the line profiles (Fig. 6b,d,f,h) recorded from the images (Fig. 6a,c,e,g). The pristine multilayers had a thickness of 19.4 nm (Fig. 6a,b) in a dry state, which was not significantly changed after UV-illumination (21.2 nm, Fig. 6c,d). The multilayers were swollen in water, with values of 28.3 nm and 51.9 nm for the pristine (Fig. 6e,f) and UV-illuminated ones (Fig. 6g,h), respectively. The significantly enhanced swelling ratio after UV illumination than the pristine one (2.45 over 1.46) reveals that the crosslinking density of the multilayers is decreased due to the breakup of the hydrophobic micellar cores, which function as the super crosslinking points for the multilayers and hence whose release enables free motion of the chain segments. Meanwhile, the excess carboxyl groups generated in such a process offer larger charge repelling in the multilayers, leading to the increase of swelling ratio too.

It has to be mentioned that the thickness of the multilayer film, no matter in a dry state or under water, was far thinner than the theoretical one (by multiplying the scale of micelles and layer numbers). This is likely due to the strong conformational restriction induced by the static electric forces and the fact that the micelles intersect with each others when adsorbed on substrates. The free chain segmentation generated in such a process can influence not only the swelling behavior but also the surface wettability by exposing more hydrophilic carboxyl groups to surface, as revealed by the significant decrease of static water contact angle from 78 ° to around 52 ° after UV-irradiation (Fig. 7).

3.4 Cell behaviors on the photoresponsive multilayers

The change of surface roughness, wettability and chemical composition may bring some unexpected influence on cellular behaviors, because cells are sensitive to these factors. To assess the cellular response, A549 and HepG2 cells were cultured on the pristine and photo-irradiated multilayers. On both types of surfaces, the cells could well attach with good viability (Fig. 8). Quantitative counting of the cell numbers, however, shows that both A549 and HepG2 cells attached onto the UV-illuminated multilayers with significantly faster rates (p<0.05), leading to the values of 141% and 152% of those of their pristine multilayers, respectively.

It is known that the organization and distribution of actin fibers can reflect the adhesion conditions of cells [29, 30]. As illustrated in the CLSM images in Fig. 9, most of the A549 on the pristine multilayers (Fig. 9a,c) had round morphology with less spreading, suggesting the weaker interaction between the cells and the substrate at this very initial stage (4 h). By contrast, on the UV-illuminated surface (Fig. 9b,d), there were more cellular pseudopod extension and actin fibers, showing stressed actin fibers and rather spreading cell morphology which are the sign of stronger cell-substrate interaction. The HepG2 were mostly in a round shape, whose actin fibers were distributed near membrane rather than in cytoplasm on the pristine multilayers (Fig. 9e,g). However, on the UV-illuminated surface (Fig. 9f,h) the cells were angulate, and the actin fibers were thicker and largely spread in cytoplasm. All these results confirm that the UV-illuminated surface can enhance the cell-substrate interaction, leading to a faster cell adhesion at the very initial stage.

Cell adhesion to biomaterial is a complicated procedure, and is influenced by various factors of materials, including the surface morphology, chemical composition, wettability, charge and so on [31, 32]. The minor increase of surface roughness after UV-irradiation, although nearly 3 times higher in the absolute value, is unlikely to have a primary effect due to the undersized magnitude compared to roughness change of micro or sub-micro meters reported in literatures [33, 34]. The UV illumination generates both extra carboxylic groups and pyrenemethanol, which are supposed to form a

phase-separated microstructure on the surface, and thereby may benefit the faster cell adhesion [35]. Higher density of carboxyl groups can lead to the promotion of cell adhesion as well [36-38]. Moreover, the increased density of carboxyl groups also decreased water contact angle from 78 ° to 52 °, which is regarded as more suitable for cell adhesion [36, 39, 40].

Although the initial cell adhesion was enhanced on the UV-irradiated multilayers, the cell proliferation on both types of surfaces showed no significant difference for both the A549 and HepG2 cells over a period of 5 d (p>0.05) (Fig. 10). Both the A549 and HepG2 cells proliferated almost linearly on both the pristine and UV-illuminated multilayers, revealing the very good cytocompatibility of the PAH/P(PA-co-AA) micelles multilayers regardless of the UV-treatment. The relative faster proliferation of A549 cells than HepG2 cells should be attributed to the nature of the cells. The reason for the difference in cell adhesion and proliferation can be explained by the different experimental protocol: the unattached cells were washed away before measuring the cell adhesion number at 4 h, while the cell viability was measured at least 1 d later. It is indeed that 1 d is long enough to achieve similar cell adhesion as shown in Fig. 10, and hence the later cell proliferation is not affected.

4. Conclusions

The photo-responsive multilayers containing UV responsive micelles were successfully prepared by assembling P(PA-co-AA) micelles and PAH on planar substrates in a layer-by-layer manner. The P(PA-co-AA) was prepared by copolymerization of pyrenemethyl acrylate and acryloyl chloride (AC), and formed micelles spontaneously in aqueous solution with an average size of 27.5 nm in a dry state and 136.6 nm in a wet state. After UV illumination, the micelles were broke up and transformed into irregular aggregates. The micelles in the multilayers could be similarly decomposed, which took place in a very fast rate, and 300 s was long enough to decompose almost completely the micelles in the multilayers. UV-irradiation led to the increase of surface roughness, enhanced wettability and swelling ratio of the multilayers. As a result, A549 and HepG2 cells showed significantly better adhesion at 4 h on the UV-illuminated multilayers, whereas the cell proliferation was not affected until 5 d. These results highlight an efficient bottom-up method for mediating structures and properties of photo-responsive multilayers, and thereby some basic cellular behaviors such as adhesion, shedding a light on their essential functions in biomedical field as surface coating on different types of materials and devices.

Acknowledgements

This study is financially supported by the Natural Science Foundation of China (21434006, 21374097), the National Key Research and Development Program of China (2016YFC1100403), the 111 Project of China (B16042), and the Fundamental Research Funds for the Central Universities (2017XZZX001-03A, 2017XZZX008-05).

References:

1 Xu, L., Y. Wang, G. Wei. Ordered DNA-Surfactant Hybrid Nanospheres Triggered by Magnetic Cationic Surfactants for Photon- and Magneto-Manipulated Drug Delivery and Release. *Biomacromolecules*, 2015. 16: 4004-4012.

2 Olejniczak, J., C. Carling, A. Almutairi. Photocontrolled release using one-photon absorption of visible or NIR light. *Journal of Controlled Release*, 2015. 219: 18-30.

3 Wang, X., J. Hu, G. Liu. Reversibly Switching Bilayer Permeability and Release Modules of Photochromic Polymersomes Stabilized by Cooperative Noncovalent Interactions. *Journal of the American Chemical Society*, 2015. 137: 15262-15275.

4 Schattling, P., F.D. Jochum, P. Theato. Multi-stimuli responsive polymers - the all-in-one talents. *Polymer Chemistry*, 2014. 5: 25-36.

5 Li, Y., H. Dong, K. Wang. Stimulus-responsive polymeric nanoparticles for biomedical applications. *Science China Chemistry*, 2010. 53: 447-457.

6 Kim, Y., Y.T. Matsunaga. Thermo-responsive polymers and their application as smart biomaterials. *Journal of Materials Chemistry B*, 2017. 5: 4307-4321.

7 Barhoumi, A., Q. Liu, D.S. Kohane. Ultraviolet light-mediated drug delivery: Principles, applications, and challenges. *Journal of Controlled Release*, 2015. 219: 31-42.

8 Pan, G.Q., B.B. Guo, Y. Ma. Dynamic Introduction of Cell Adhesive Factor via Reversible Multicovalent Phenylboronic Acid/cis-Diol Polymeric Complexes. *Journal of the American Chemical Society*, 2014. 136: 6203-6206.

9 Lu, Y., A.A. Aimetti, R. Langer. Bioresponsive materials. *Nature Reviews Materials*, 2016. 1: 16075.

10 Rodrigo-Navarro, A., P. Rico, A. Saadeddin. Living biointerfaces based on non-pathogenic bacteria to direct cell differentiation. *Scientific Reports*, 2014. 4: 5849.

11 Wang, H., W. Zhang, C. Gao. Shape Transformation of Light-Responsive Pyrene-Containing Micelles and Their Influence on Cytoviability. *Biomacromolecules*, 2015. 16: 2276-2281.

12 Zhao, Y. Light-Responsive Block Copolymer Micelles. *Macromolecules*, 2012. 45: 3647-3657.

13 Schumers, J., C. Fustin, J. Gohy. Light-Responsive Block Copolymers. *Macromolecular Rapid Communications*, 2010. 31: 1588-1607.

14 Decher, G. Fuzzy Nanoassemblies: Toward Layered Polymeric Multicomposites. *Science*, 1997. 277: 1232.

15 Liang, S., N. Zhou, S. Yu. Buildup of hyperbranched polymer/alginate multilayers and their influence on protein adsorption and platelet adhesion. *Journal of Applied Polymer Science*, 2017. 134.

16 Kharlampieva, E., S.A. Sukhishvili. Hydrogen‐Bonded Layer‐by‐Layer Polymer Films. *Journal of Macromolecular Science, Part C*, 2006. 46: 377-395.

17 Kotov, N.A. Layer-by-layer self-assembly: The contribution of hydrophobic interactions. *Nanostructured Materials*, 1999. 12: 789-796.

18 Tang, Z., Y. Wang, P. Podsiadlo. Biomedical Applications of Layer-by-Layer Assembly: From Biomimetics to Tissue Engineering. *Advanced Materials*, 2006. 18: 3203-3224.

19 Guo, S., X. Zhu, X.J. Loh. Controlling cell adhesion using layer-by-layer approaches for biomedical applications. *Materials Science & Engineering C-Materials for Biological Applications*, 2017. 70: 1163-1175.

20 Chen, Y., R. Zhu, Z. Xu. Self-assembly of pifithrin-alpha-loaded layered double hydroxide/chitosan nanohybrid composites as a drug delivery system for bone repair materials. *Journal of Materials Chemistry B*, 2017. 5: 2245-2253.

21 Zhang, D., C. Jiang, J. Liu. Carbon monoxide gas sensing at room temperature using copper oxide-decorated graphene hybrid nanocomposite prepared by layer-by-layer self-assembly. *Sensors and Actuators B-Chemical*, 2017. 247: 875-882.

22 Manmuanpom, N., S.T. Dubas, S. Wongkasemjit. Layer-by-layer modification of porous polybenzoxazine with silver nanoparticles for enhanced CO2 storage. *Journal of Applied Polymer Science*, 2017. 134.

23 Yusan, P., I. Tuncel, V. Butun. pH-responsive layer-by-layer films of zwitterionic block copolymer micelles. *Polymer Chemistry*, 2014. 5: 3777-3787.

24 Zhu, Z., S.A. Sukhishvili. Layer-by-layer films of stimuli-responsive block copolymer micelles. *Journal of Materials Chemistry*, 2012. 22: 7667-7671.

25 Li, Y., X. Li, W. Guo. Spontaneous wrinkling of layer-by-layer assembled polyelectrolyte films for humidity-responsive superhydrophobicity. *Science China Chemistry*, 2016. 59: 1568-1573.

26 Gensel, J., I. Dewald, J. Erath. Reversible swelling transitions in stimuli-responsive layer-by-layer films containing block copolymer micelles. *Chemical Science*, 2013. 4: 325-334.

27 Zhu, Z., S.A. Sukhishvili. Temperature-Induced Swelling and Small Molecule Release with Hydrogen-Bonded Multilayers of Block Copolymer Micelles. *ACS Nano*, 2009. 3: 3595-3605.

28 Bieker, P., M. Schoenhoff. Linear and Exponential Growth Regimes of Multi layers of Weak Polyelectrolytes in Dependence on pH. *Macromolecules*, 2010. 43: 5052-5059.

29 Le Clainche, C., M. Carlier. Regulation of actin assembly associated with protrusion and adhesion in cell migration. *Physiological Reviews*, 2008. 88: 489-513.

30 Zimmer, C.C., L. Shi, Y. Shih. F-Actin reassembly during focal adhesion impacts single cell mechanics and nanoscale membrane structure. *Science China Chemistry*, 2012. 55: 1922-1930.

31 Yuan, W., N. Zhao, B. Yu. Thermo-responsive gelatin-functionalized PCL film surfaces for improvement of cell adhesion and intelligent recovery of gene-transfected cells. *Science China Chemistry*, 2014. 57: 586-595.

32 Liu, H., S. Wang. Poly(N-isopropylacrylamide)-based thermo-responsive surfaces with controllable cell adhesion. *Science China Chemistry*, 2014. 57: 552-557.

33 Lampin, M., R. WarocquierClerout, C. Legris. Correlation between substratum roughness and wettability, cell adhesion, and cell migration. *Journal of Biomedical Materials Research*, 1997. 36: 99-108.

34 Ranella, A., M. Barberoglou, S. Bakogianni. Tuning cell adhesion by controlling the roughness and wettability of 3D micro/nano silicon structures. *Acta Biomaterialia*, 2010. 6: 2711-2720.

35 Zapata, P., J. Su, A.J. Garcia. Quantitative high-throughput screening of osteoblast attachment, spreading, and proliferation on demixed polymer blend micropatterns. *Biomacromolecules*, 2007. 8: 1907-1917.

36 Hwang, I., M. Oh, C. Jung. Direct patterning of poly(acrylic acid) on polymer surfaces by ion beam lithography for the controlled adhesion of mammalian cells. *Biotechnology Letters*, 2014. 36: 2135-2142.

37 Li, B., Y. Ma, S. Wang. Influence of carboxyl group density on neuron cell attachment and differentiation behavior: Gradient-guided neurite outgrowth. *Biomaterials*, 2005. 26: 4956-4963.

38 Faucheux, N., R. Schweiss, K. Lützow. Self-assembled monolayers with different terminating groups as model substrates for cell adhesion studies. *Biomaterials*, 2004. 25: 2721-2730.

39 Bet, M.R., G. Goissis, S. Vargas. Cell adhesion and cytotoxicity studies over polyanionic collagen surfaces with variable negative charge and wettability. *Biomaterials*, 2003. 24: 131-137.

40 Arima, Y., H. Iwata. Effect of wettability and surface functional groups on protein adsorption and cell adhesion using well-defined mixed self-assembled monolayers. *Biomaterials*, 2007. 28: 3074-3082.

Figure Captions:

Scheme 1 Chemical structure of P(PA-co-AA) copolymer and its decomposition under UV irradiation (a). Illustration of structure change of multilayers under UV irradiation and their influence on cell adhesion.

Figure 1 ^{1}H NMR spectra (a) of pyrenemethyl acrylate and P(PA-co-AA) measured in DMSO-d_6. (b) FT-IR spectra of P(PA-co-AA) copolymers, PA and AA.

Figure 2 TEM images of photo responsive micelles before (a) and after UV irradiation at 50 mW for 0.5 h (b). Insets are higher magnification images. Scale bars represent 500 nm. Statistic histograms of micelle sizes before (c) and after (d) UV irradiation.

Figure 3 (a) Absorbance of multilayers in 250-400 nm with different bilayer numbers. (b) Absorbance at 343 nm as a function of bilayer number.

Figure 4 (a) Absorbance of pristine, ethanol treated, and UV irradiated for 30 s and ethanol treated multilayers in 250-400 nm. (b) Absorbance of the multilayers at 343 nm as a function of UV irradiation time. The irradiate multilayers were thoroughly washed with ethanol before measurement.

Figure 5 AFM images of pristine (a) and UV-irradiated multilayers (b).

Figure 6 AFM images (a, c, e, g) and line profiles (b, d, f, h) of multilayers before (a, b, e, f) and after (c, d, g, h) UV irradiation for 300s measured in a dry state (a-d) and under Milli-Q water (e-h), respectively.

Figure 7 Water contact angles of pristine (a) and UV-irradiated multilayers (b). (c) Statistical analysis of contact angles. 3 independent experiments were carried out. * indicates statistically significant difference at $p < 0.05$ level.

Figure 8 Representative fluorescent images of A549 (a, c) and HepG2 cells (b, d) being cultured on pristine (a, b) and UV-irradiated (c, d) multilayers. Scale bars represent 50 μm. (e) Adhesion numbers of A549 and HepG2 cells after being cultured for 4 h with a seeding density of 1.1×10^4 cells/cm^2. At least 10 images were analyzed for each sample and 3 independent experiments were carried out. * indicates statistically significant difference at $p < 0.05$ level.

Figure 9 CLSM images of A549 (a-d) and HepG2 (e-h) cells after being cultured on pristine (a, c, e, g) and UV-irradiated (b, d, f, h) multilayers for 4h with a seeding density of 1.1×10^4 cells/cm^2. F-actin (red) and nucleus (blue) were stained with rhodamine-labeled phalloidin and DAPI, respectively. Scale bars represent 20 μm.

Figure 10 Viability of A549 and HPG2 cells seeded on different surfaces for 1, 3 and 5 d. 3 independent experiments were carried out for each group. * indicates statistically significant difference at $p < 0.05$ level.

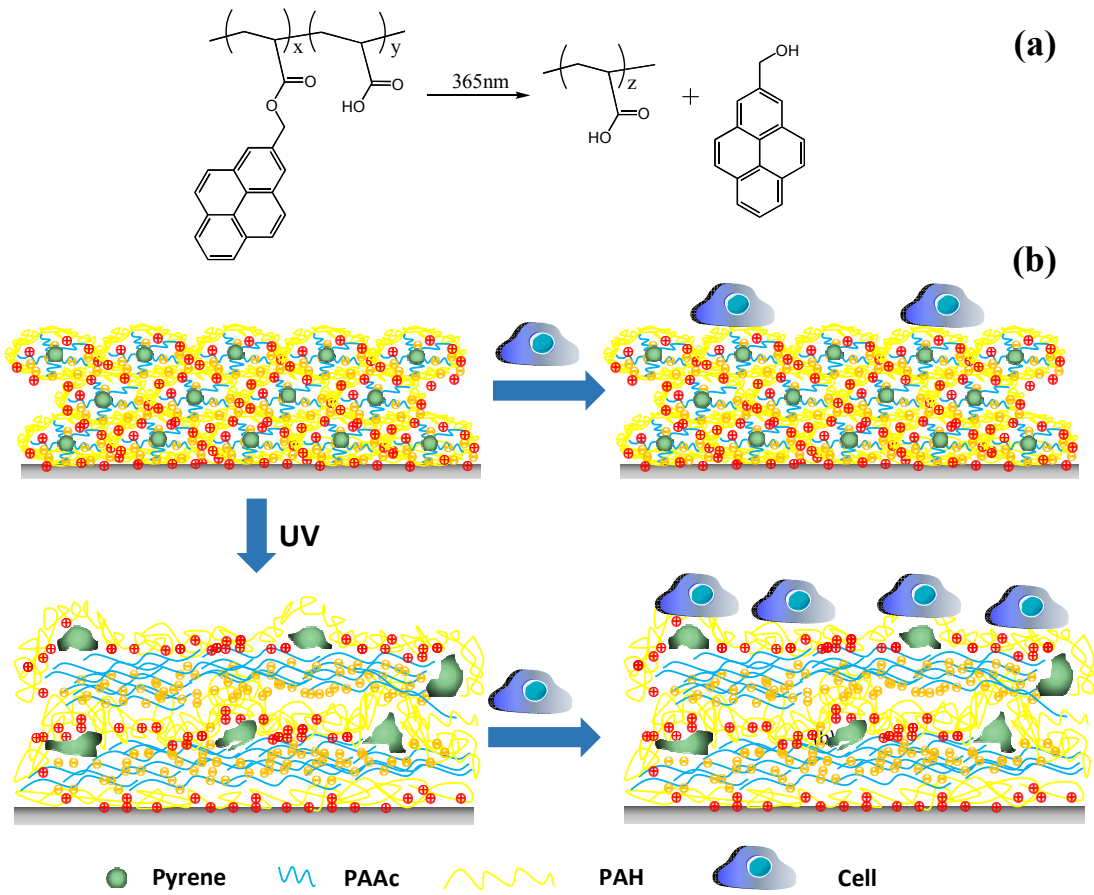

Scheme 1

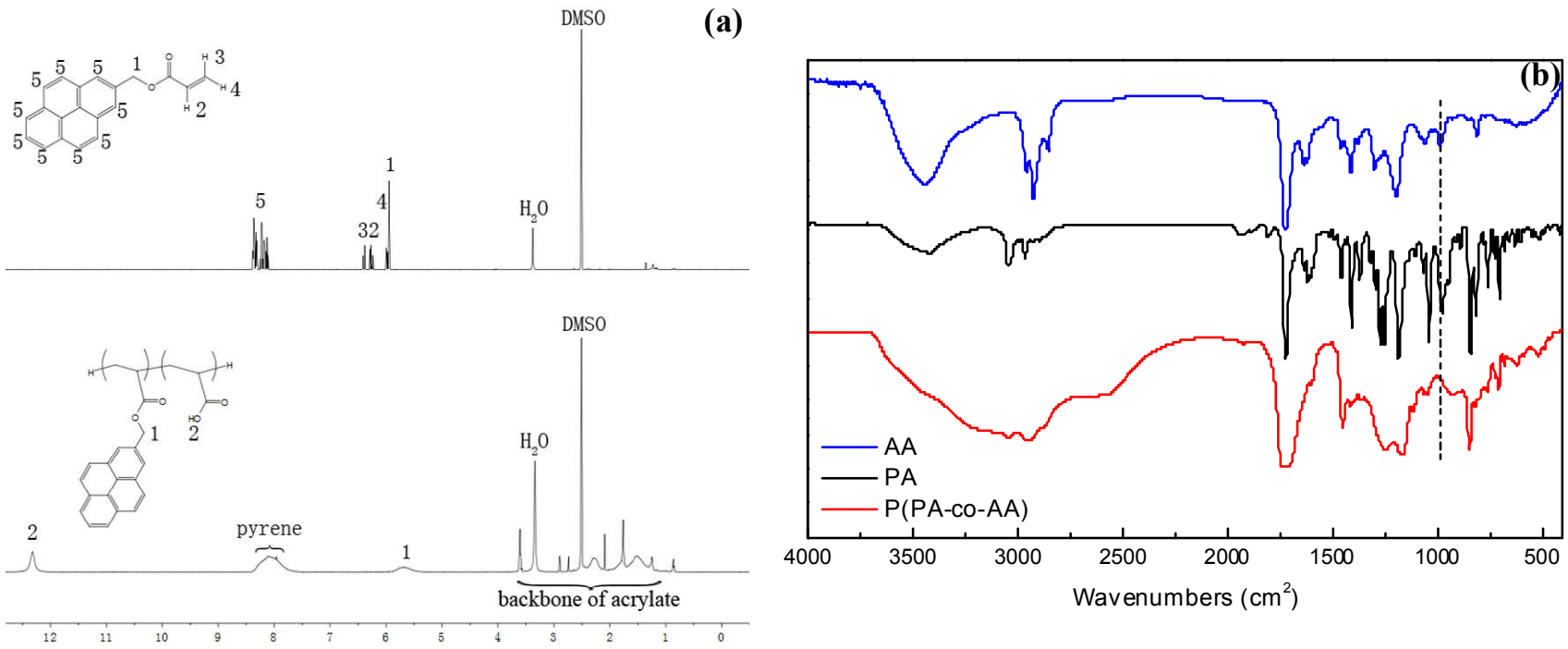
(a)
DMSO
H2O
5
4
32
1
DMSO
H2O
pyrene
backbone of acrylate
2
1
(b)
AA
PA
P(PA-co-AA)
4000
3500
3000
2500
2000
1500
1000
500
Wavenumbers (cm2)

Figure 1

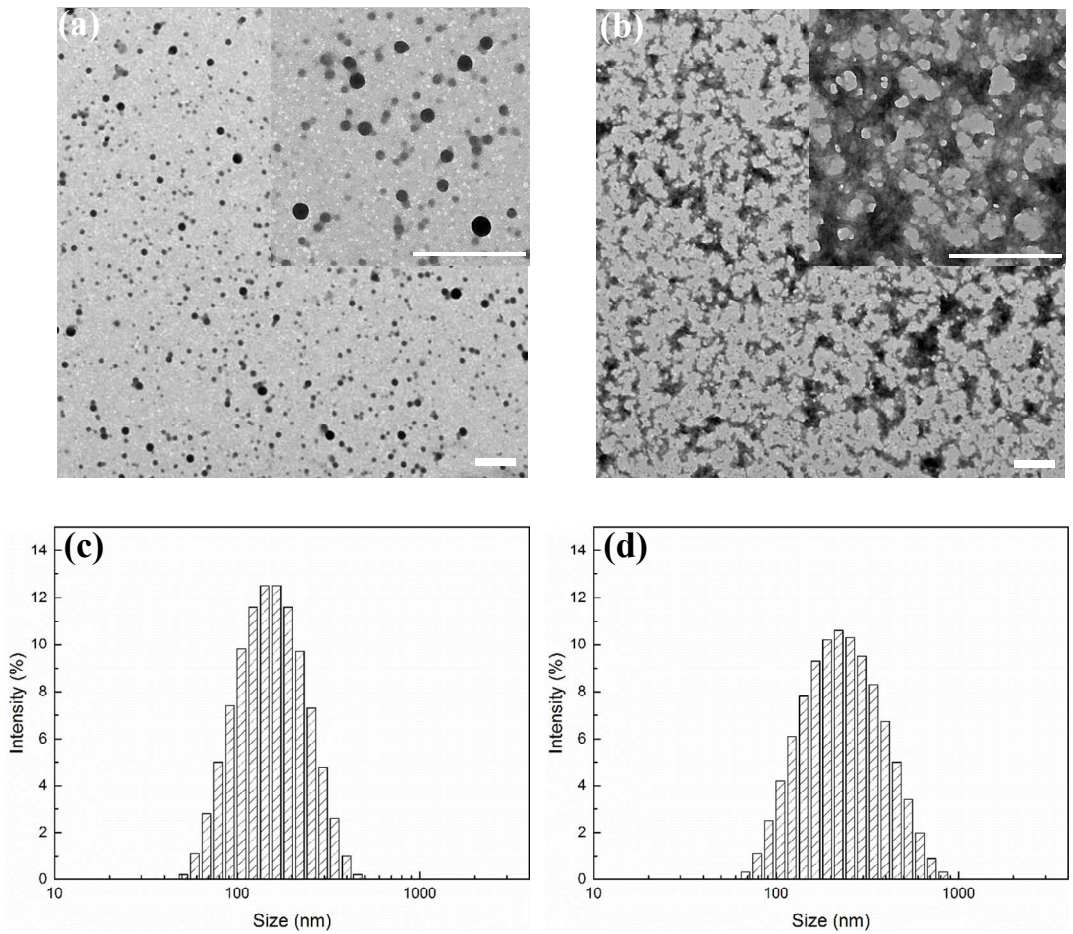

Figure 2

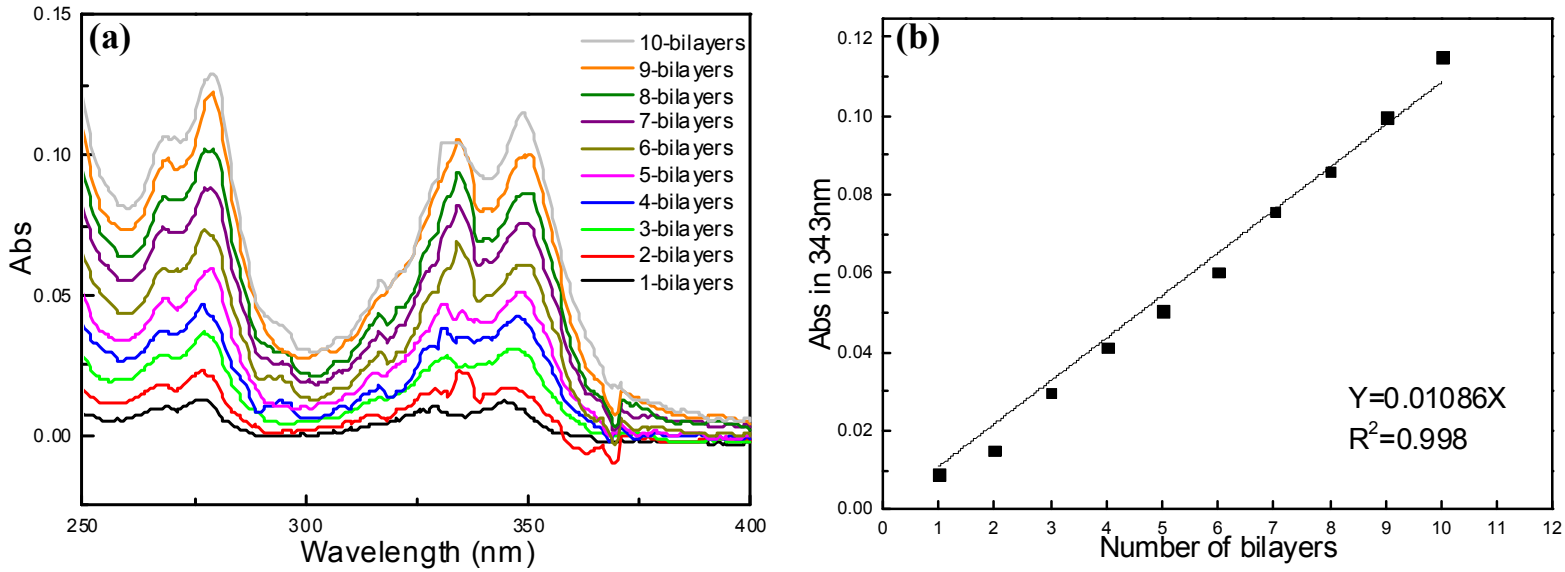
(a)
10-bilayers
9-bilayers
8-bilayers
7-bilayers
6-bilayers
5-bilayers
4-bilayers
3-bilayers
2-bilayers
1-bilayers
Abs
Wavelength (nm)
0.15
0.10
0.05
0.00
250
300
350
400
(b)
Abs in 343nm
Number of bilayers
Y=0.01086X
R2=0.998
0.12
0.10
0.08
0.06
0.04
0.02
0.00
0
1
2
3
4
5
6
7
8
9
10
11
12

Figure 3

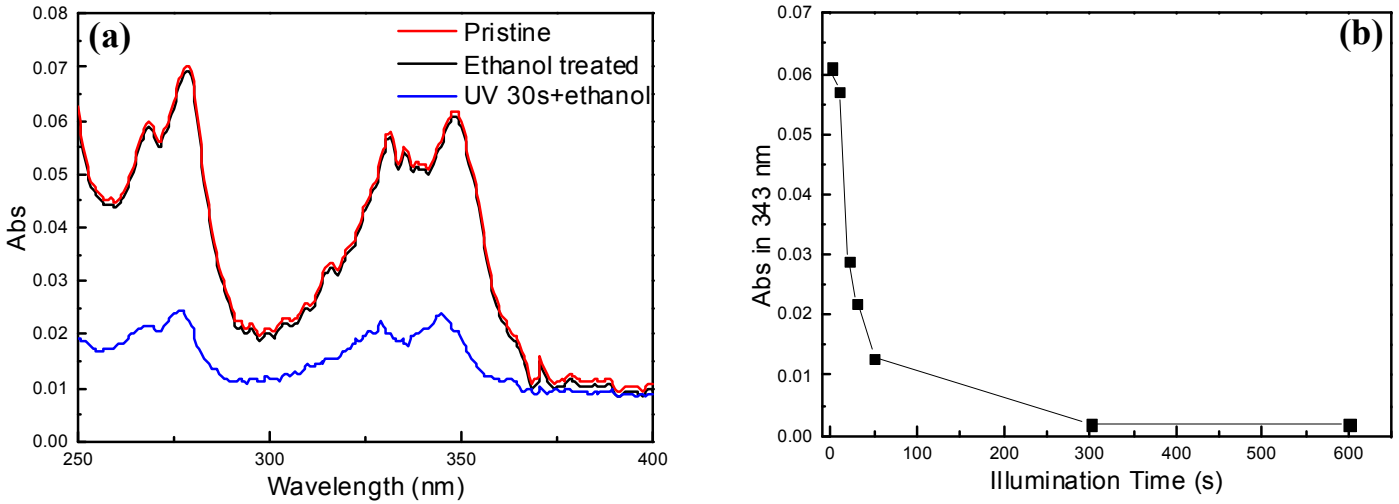
(a)
Pristine
Ethanol treated
UV 30s+ethanol
Abs
Wavelength (nm)
0.00
0.01
0.02
0.03
0.04
0.05
0.06
0.07
0.08
250
300
350
400
(b)
Abs in 343 nm
Illumination Time (s)
0
100
200
300
400
500
600

Figure 4

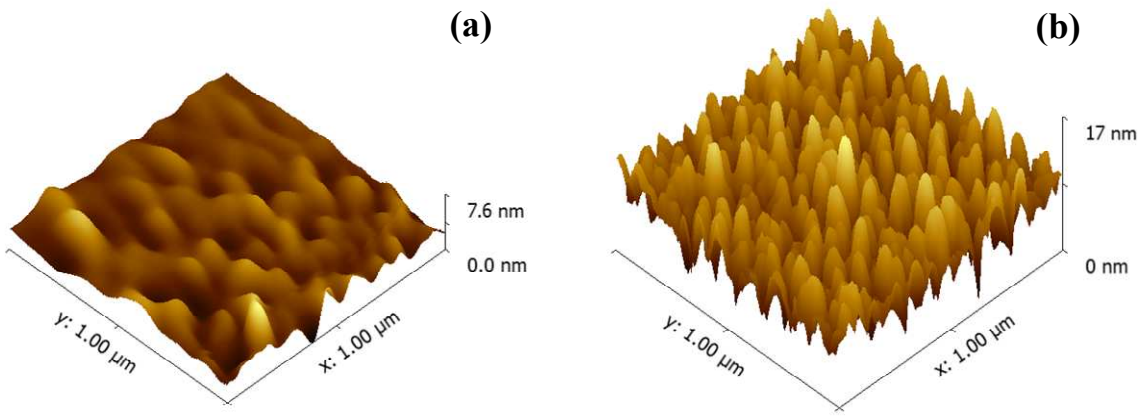

Figure 5

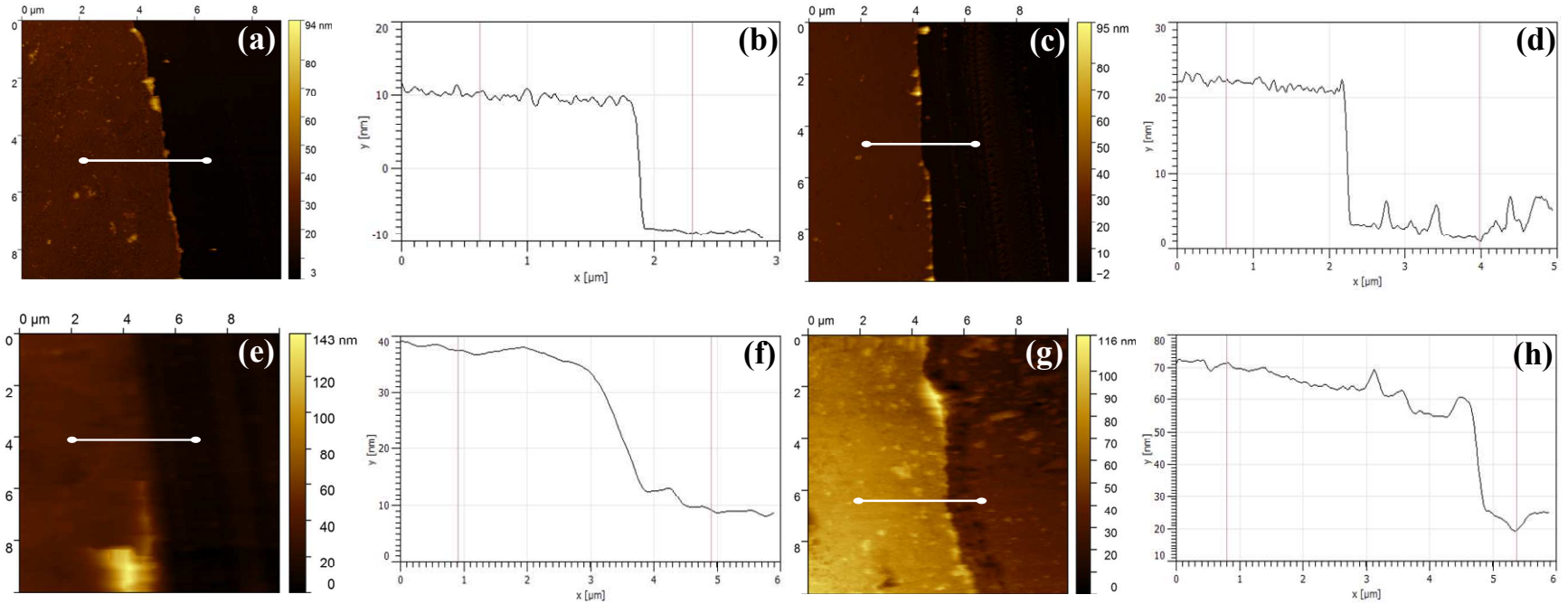

Figure 6

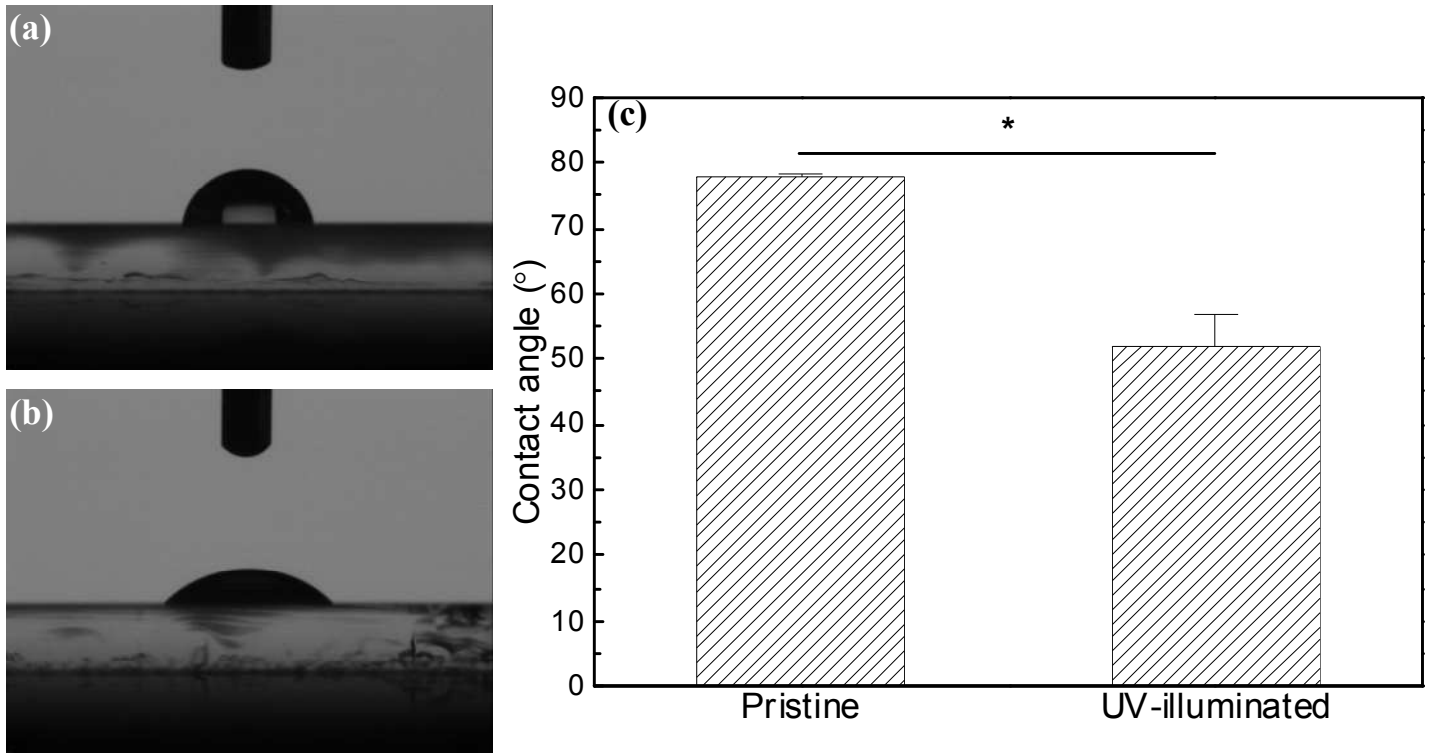
(a)
(b)
(c)
*
Contact angle (°)
0
10
20
30
40
50
60
70
80
90
Pristine
UV-illuminated

Figure 7

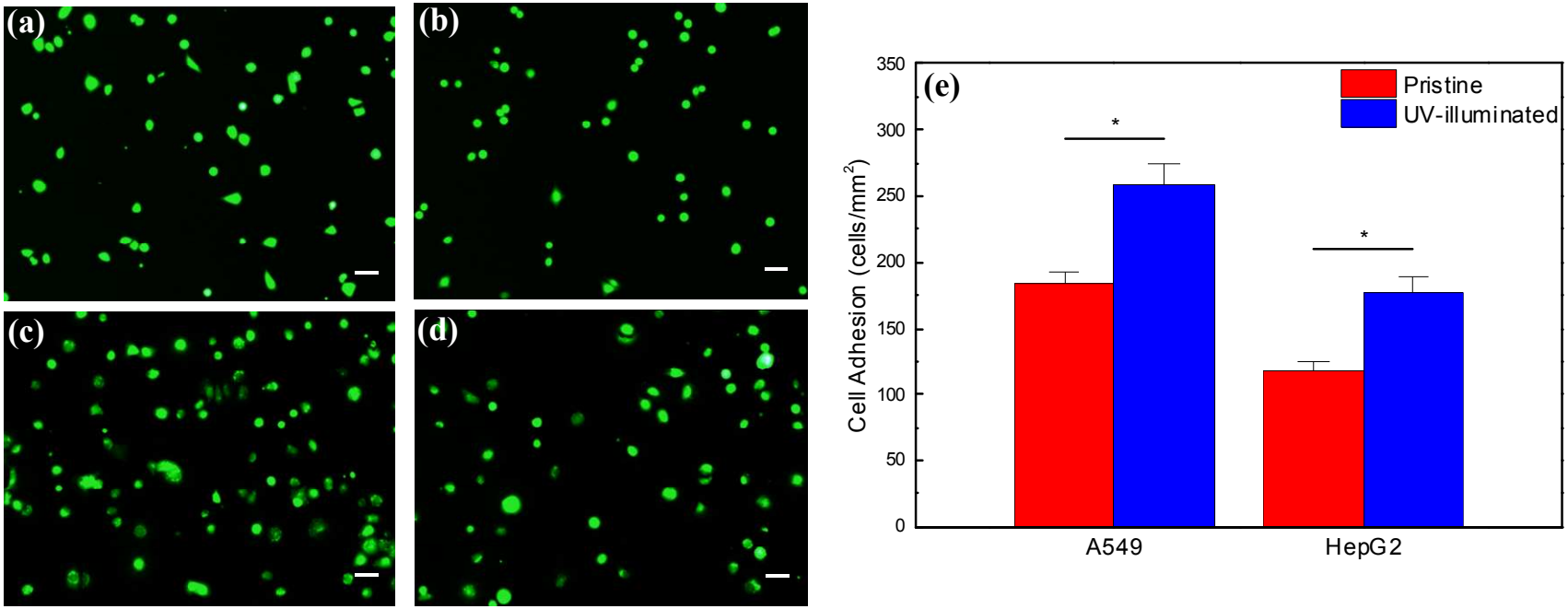
(a)
(b)
(c)
(d)
(e)
Pristine
UV-illuminated
Cell Adhesion (cells/mm2)
350
300
250
200
150
100
50
0
*
*
A549
HepG2

Figure 8

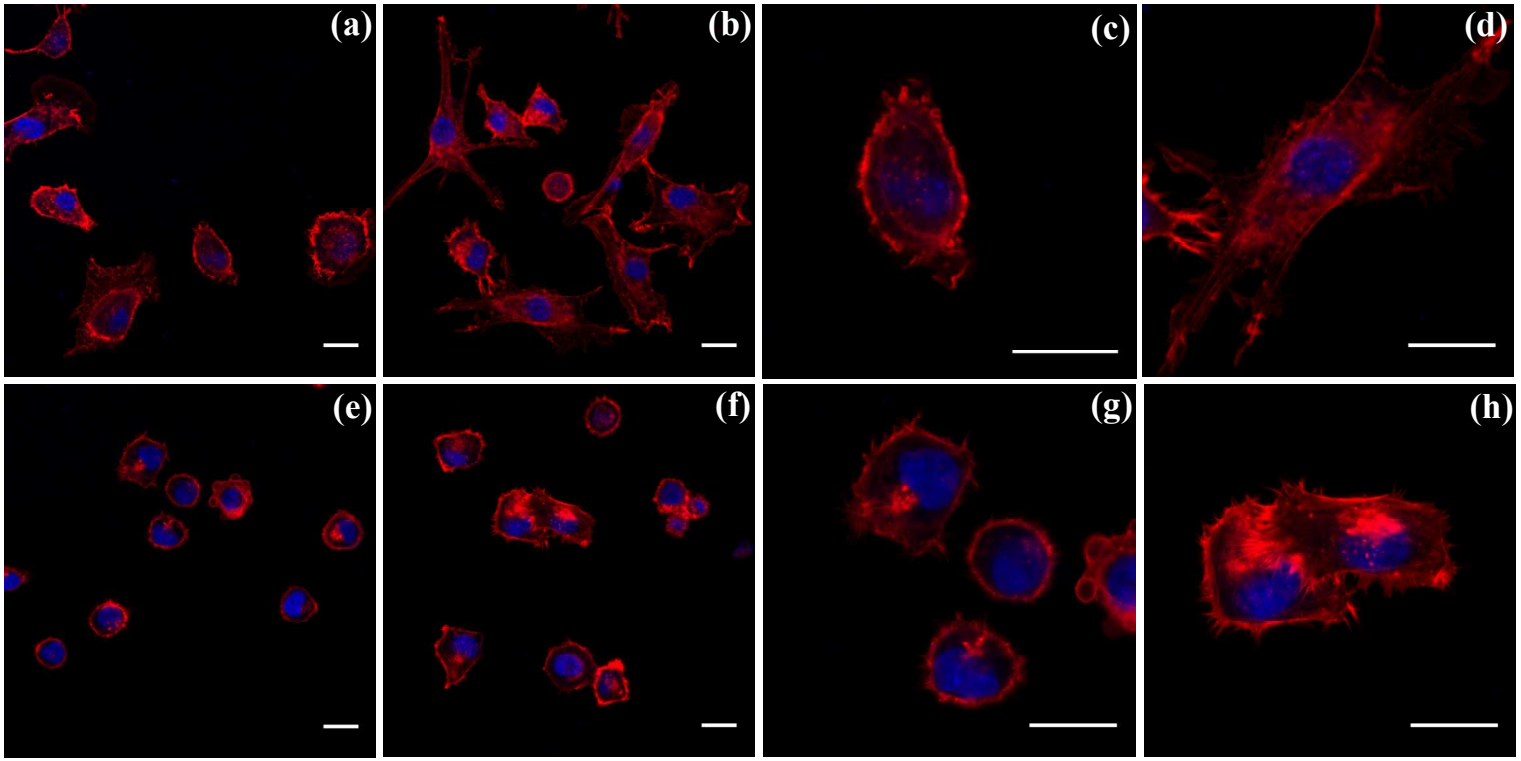

Figure 9

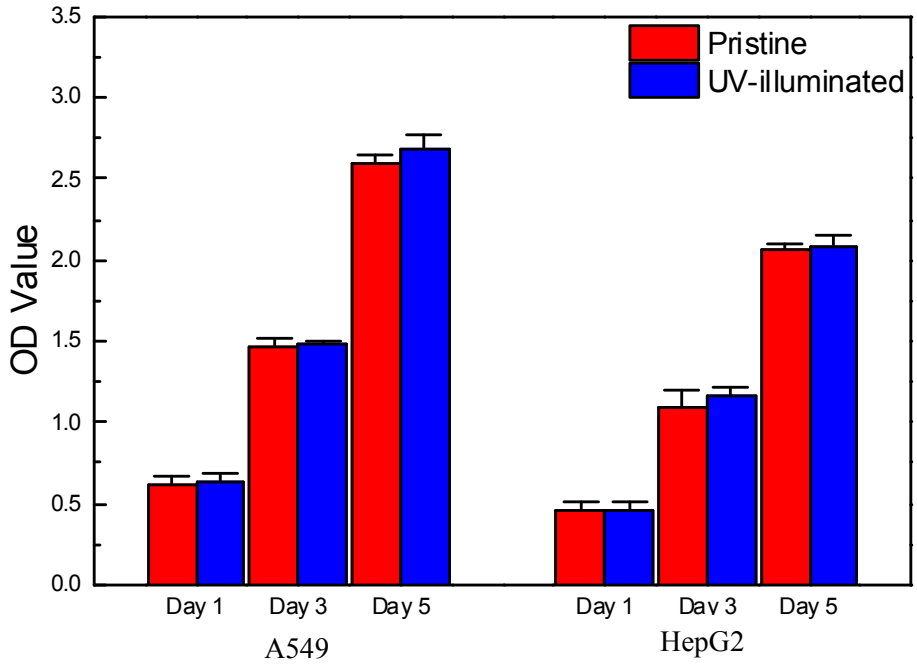
3.5
3.0
2.5
2.0
1.5
1.0
0.5
0.0
OD Value
Pristine
UV-illuminated
Day 1
Day 3
Day 5
A549
Day 1
Dav 3
Day 5
HepG2

Figure 10